Towards an Efficient 3D Numerical Wave Tank using the Harmonic Polynomial Cell method with Adaptive Grid Refinement

Finn-Christian Wickmann Hanssen[1,*], Marilena Greco[1,2], Jens B. Helmers[3], Yanlin Shao[4,5]

[1]NTNU AMOS, Department of Marine Technology, NTNU, Trondheim, Norway
[2]CNR-INM, Institute of Marine Engineering, Rome, Italy
[3]Department of Ship Hydrodynamics, DNV, Oslo, Norway
[4]Department of Mechanical Engineering, DTU, Lyngby, Denmark
[5]College of Shipbuilding Engineering, Harbin Engineering University, Harbin, China
[*]finnchri83@gmail.com

1 Introduction

An extension from 2D to 3D of the fully-nonlinear numerical wave tank (NWT) used by Hanssen et al. [1] is presented. Potential-flow theory is assumed, and the high-order harmonic polynomial cell (HPC) field method proposed by Shao and Faltinsen [2] is used to solve the governing Laplace equation for the velocity potential φ numerically. The present work deals with an immersed boundary method without and with the use of an octree technique for local grid refinement near the air-water interface, and examines only wave propagation; dealing with wave-body interactions is planned as a future development. Figure 1 (a) illustrates the physical domain bounded by a free surface S_{FS}, vertical tank sides S_{TS} and a flat seabed S_{SB} where the hydrodynamic boundary-value problem (BVP) for φ is solved. S_{FS} is modelled as an immersed boundary in a stationary Cartesian grid with overlapping cells. As shown in Figure 1 (b), the cells consist of 26 boundary nodes and are characterized by the node spacing $(\Delta x, \Delta y, \Delta z)$. Each cell has a local $o\overline{xyz}$ coordinate system with origin in the interior node. For an arbitrary point, the relationship between the global and local coordinate systems is $\overline{\boldsymbol{x}} = \boldsymbol{x} - \boldsymbol{x}_{27}$, where $\boldsymbol{x}_{27}$ are the global coordinates of the interior cell node. Everywhere inside a cell the velocity potential is represented as

$$\varphi(\overline{\boldsymbol{x}}) = \sum_{i=1}^{26} b_i(\overline{\boldsymbol{x}})\varphi_i; \quad \overline{\boldsymbol{x}} \in \{|\overline{x}| \leq \Delta x \wedge |\overline{y}| \leq \Delta y \wedge |\overline{z}| \leq \Delta z\}, \tag{1}$$

where $\varphi_i, i = 1, ..., 26$ are the values of the velocity potential in the boundary nodes and $b_i, i = 1, ..., 26$ are smoothly-varying coefficients involving the same set of harmonic polynomials as used by Shao and Faltinsen [2].

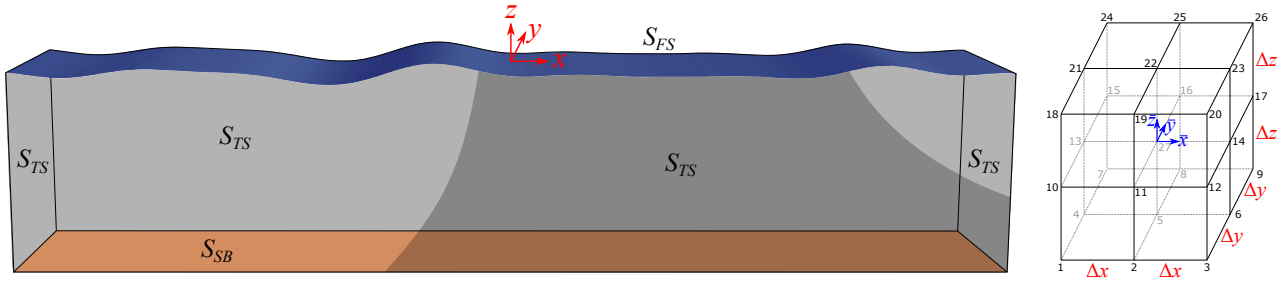

(a) Numerical wave tank (b) Cubic cell

Figure 1: Definition of hydrodynamic BVP in a global $Oxyz$ coordinate system (a) and a cubic cell with a local $o\overline{xyz}$ coordinate system (b).

S_{SF} is described by semi-Lagrangian markers with horizontal coordinates coinciding with the grid nodes and that only move vertically. It is noted, however, that the method can be modified to allow for fully-Lagrangian markers. The global matrix of the algebraic equation system for φ is obtained using equation (1) to enforce Dirichlet conditions on S_{SF}, the spatial derivative of the same equation to enforce Neumann conditions on S_{TS} and S_{SB}, and a continuity equation for interior nodes below S_{SF} obtained by using equation (1) to express φ in $\overline{\boldsymbol{x}} = \boldsymbol{0}$ for all cells. When we introduce octree grids to locally refine the solution close to S_{SF}, some of the continuity equations are modified to implicitly couple the numerical solution in different octree-grid levels.

The rest of the paper is organized as follows: First, the local solution properties in an arbitrary cell are investigated to give guidance on proper modelling strategies. Thereafter, the accuracy and efficiency of the solution for a realistic global BVP are looked into. Finally, conclusions are drawn and future work outlined.

2 Local Solution Properties in a Cell

Investigating the fundamental properties of the HPC method in 2D, Ma et al. [3] found that in order to maximize the accuracy of the numerical solution, undistorted, square cells should be used. The accuracy of the numerical

solution in each cell directly influences the accuracy of the global BVP, and the numerical stability in a time-domain simulation. To examine if the findings are valid also in 3D, a similar study as in [3] is therefore performed. Analytical Dirichlet conditions are enforced in all 26 boundary nodes of a cell, and the absolute error of the numerical solution is computed in the position of the interior node (node 27 in Figure 1 (b)). As analytical solution we use the wave-like expression $\varphi_{ana}(\overline{\boldsymbol{x}}) = [\omega\zeta_A \cosh k(\overline{z}+h)\sin\theta]/[k\sinh kh]$ with $\theta = k\overline{x}\cos\beta + k\overline{y}\sin\beta + \alpha$ and $\omega = \sqrt{gk}$. The following parameters are applied: $\zeta_A = 1.0\ m$, $k = \pi/6\ m^{-1}$, $h = \pi/k$, $g = 9.81\ m/s^2$, $\beta = \pi/4$ and $\alpha = -\pi/5$. The cell's aspect ratio, describing its stretching, is defined as $\Delta x/\Delta z$, and the skewness, describing its distortion, is defined as $\cot\gamma_y = 1/\tan\gamma_y$. γ_y is the angle the straight line through nodes 5-27-22 is rotated about the y-axis. Figure 2 shows examples of a few stretched or distorted cells. The error of the numerical solution is defined as $\epsilon_\chi(\overline{\boldsymbol{x}}) = |\chi_{num}(\overline{\boldsymbol{x}}) - \chi_{ana}(\overline{\boldsymbol{x}})|/\max|\chi_{ana}|$, where $\max|\chi_{ana}|$ is the maximum absolute value of the analytical solution anywhere inside the cell and χ is either φ or any of the three components of $\nabla\varphi$. Figure 3 shows that the effect of stretching an undistorted cell, or skewing a cell with unit aspect ratio, is similar in 2D and 3D. Although the shapes and absolute values of the error curves depend on the enforced numerical solution, which naturally differ in 2D and 3D, the results are qualitatively consistent. Hence, where square, undistorted cells are required to maximize the numerical accuracy in 2D, it is equally important to use cubic, undistorted cells in 3D. This can only be achieved in Cartesian grids, which require that complex surfaces are modelled as immersed boundaries.

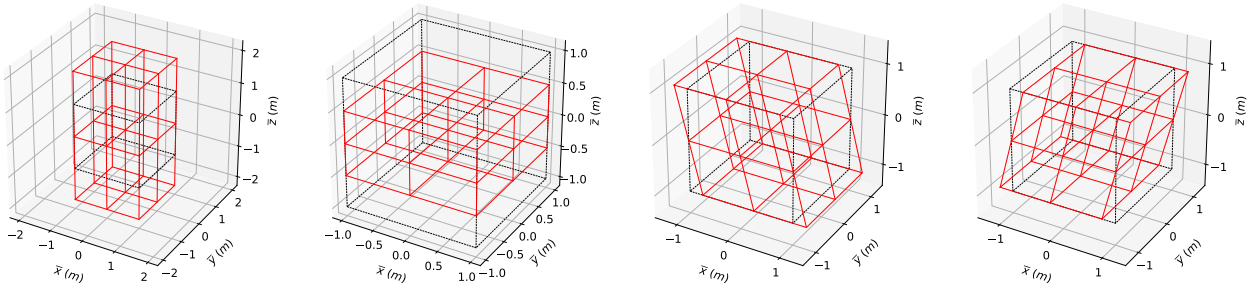

(a) $\Delta x/\Delta z = 0.5$ (b) $\Delta x/\Delta z = 2.0$ (c) $\gamma_y = -14.32°$ (d) $\gamma_y = 14.32°$

Figure 2: Examples of stretched and distorted cells. Black dashed lines indicate a cubic, undistorted cell.

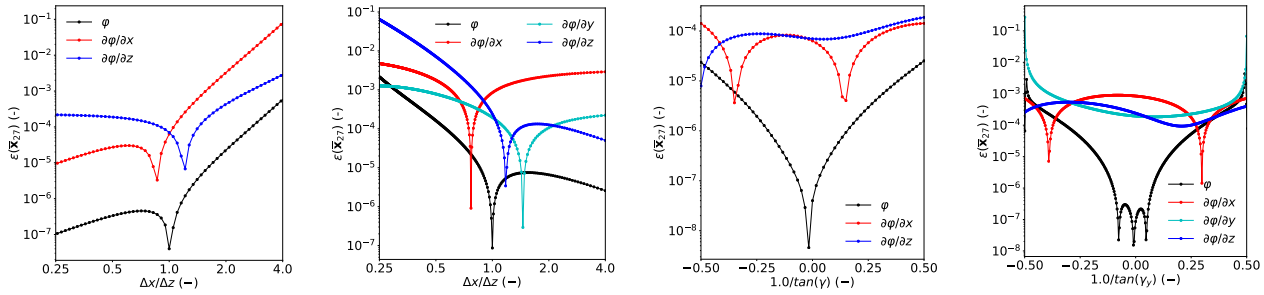

(a) Stretching (2D [3]) (b) Stretching (3D) (c) Distortion (2D [3]) (d) Distortion (3D)

Figure 3: Absolute error in the interior cell node as a function of the cell's aspect ratio and skewness.

With S_{SF} modelled as an immersed boundary, the associated free-surface Dirichlet conditions are enforced in cells intersected by S_{SF} in the upper half-plane. We here examine if the numerical accuracy is influence by where S_{SF} intersects the cell by varying $\zeta(\tilde{\boldsymbol{x}}_{27}) - z_{27}$ between 0 and Δz. The analytical Dirichlet conditions previously enforced in nodes $18-26$ are replaced with Dirichlet conditions in the position of free-surface markers with the same horizontal coordinates $\tilde{\boldsymbol{x}}$ and vertical coordinates given by the analytical wave elevation $\zeta_{ana}(\tilde{\boldsymbol{x}}, t) = \zeta_A\cos\theta$, where $\theta = kx\cos\beta + ky\sin\beta - \omega t$. The Dirichlet conditions are given by the corresponding analytical velocity potential $\varphi_{ana}(\boldsymbol{x}, t) = [\omega\zeta_A\cosh k(z+h)\sin\theta]/[k\sinh kh]$. The following parameters, realistic for a typical numerical simulation, are used: $\zeta_A = 0.2\Delta z$, $\lambda = 25\Delta x$, $\beta = \pi/4$ and $h = 0.5\lambda$. It is noted that, although the analytical solution here corresponds to a linear solution, we enforce φ_{ana} in the exact position of S_{SF} that may be above the still waterline. Figure 4 shows examples of cells intersected by S_{SF} at three different vertical positions and corresponding errors of $\partial\varphi/\partial z$ on S_{SF}. It is generally observed that the distributions of errors, both on and below S_{SF}, vary little with the vertical position of S_{SF} relative to z_{27}. The errors of $\nabla\varphi$ on S_{SF} are always moderate in the cell's interior free-surface marker compared to in the eight boundary markers. Hence, when estimating $\nabla\varphi$ for a marker as the spatial derivative of equation (1), it is recommended to use the cell where this is the interior marker whenever possible.

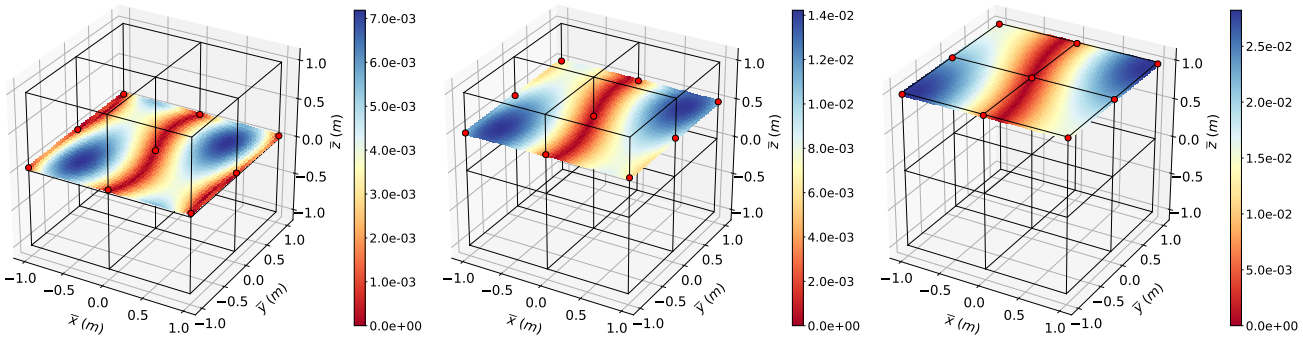

(a) Low filling (b) Intermediate filling (c) Large filling

Figure 4: Cells intersected by S_{SF} in different vertical positions at $t = 0$. The colour bars indicate numerical errors of $\partial\varphi/\partial z$ on S_{SF}. Red circles indicate free-surface markers.

3 Global Accuracy with Local Grid Refinement

Promising results using the HPC method to model a large-domain NWT in 3D were presented by Liang et al. [4], however, involving a large number of cells. Here, we introduce an octree-grid strategy to reduce the number of cells, which ultimately is required to achieve a method that is practical without the use of supercomputers. As a case study we use a third-order spectral solution for an irregular, long-crested sea state with significant wave height $H_s = 8\ m$ and peak period $T_p = 10\ s$ as reference solution to enforce boundary conditions in a NWT similar to that in Figure 1. The NWT is 500 m long and 100 m wide and with $h = 100\ m$. 2D projections of four uniform grids with different levels of local octree refinement close to the free surface are shown in Figure 5 together with resulting errors in φ and $\partial\varphi/\partial z$. $N_{levels} = 1$ corresponds to no refinement, whereas $N_{levels} = 4$ means that the grid is refined locally three times. All the grids have $\Delta x \approx \lambda_p/7.5$ in the coarsest refinement level, while $N_{levels} = 4$ gives a refinement $\Delta x \approx \lambda_p/60$ near S_{SF} where λ_p is the wavelength corresponding to T_p. Increasing N_{levels}, the numerical solution clearly becomes more accurate in the proximity of S_{SF}, while towards S_{SB} the errors are similar in all grids. The reason for not seeing zero errors on S_{SF} is that these are computed in points that generally do not coincide with free-surface markers (where Dirichlet conditions for φ are enforced).

In Figure 6 the L2 errors of φ, $\partial\varphi/\partial x$ and $\partial\varphi/\partial z$ computed over 12500 points on S_{SF} are plotted as a function of the CPU time used to solve the global BVP in Python on a standard laptop with an iterative BiCGStab solver with spilu preconditioner. For the smallest errors i.e. the most refined grids, the CPU time can be reduced with up to 100 times using the local refinement compared to a grid with $N_{levels} = 1$. Although involving some additional effort to construct the global coefficient matrix, the results indicate that the local grid-refinement technique can improve the computational efficiency substantially.

4 Conclusions

Examining the local properties of the 3D HPC method, it is recommended to use Cartesian grids with undistorted, cubic cells to maximize the accuracy of the numerical solution. This confirms the 2D findings made by

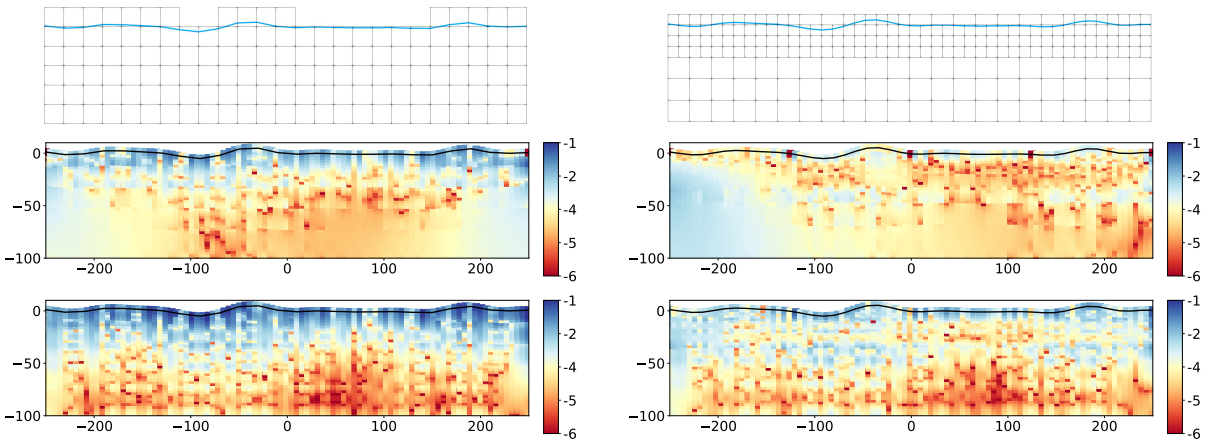

(a) $N_{levels} = 1$ (b) $N_{levels} = 2$

Figure 5: $\log_{10}(\epsilon_\varphi)$ and $\log_{10}(\epsilon_{\partial\varphi/\partial z})$ for different N_{levels}.

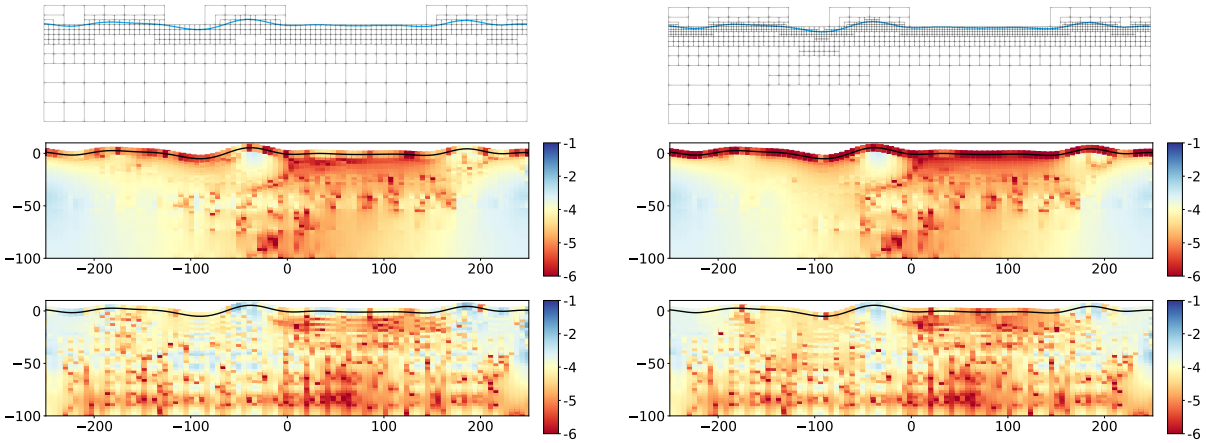

(c) $N_{levels} = 3$ (d) $N_{levels} = 4$

Figure 5: $\log_{10}(\epsilon_\varphi)$ and $\log_{10}(\epsilon_{\partial\varphi/\partial z})$ for different N_{levels} (cont.).

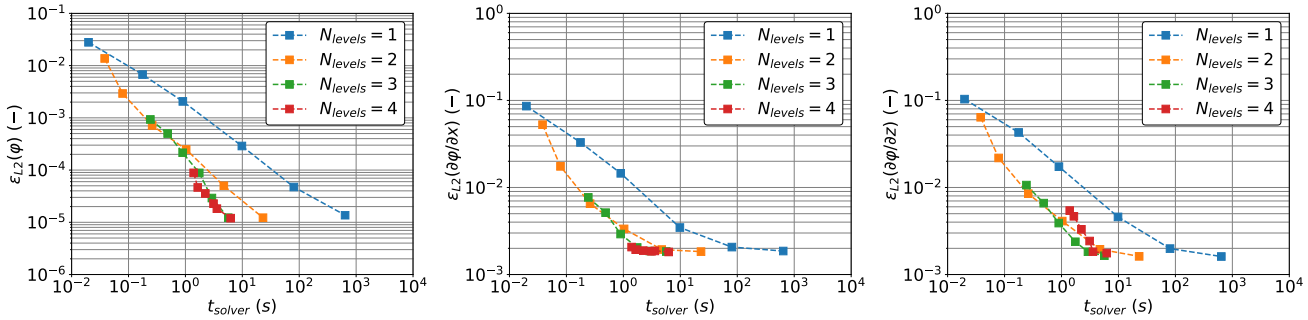

(a) $\epsilon_{L2}(\varphi)$ (b) $\epsilon_{L2}(\partial\varphi/\partial x)$ (c) $\epsilon_{L2}(\partial\varphi/\partial z)$

Figure 6: L_2 errors on the free surface plotted as a function of the CPU time used to solve the global BVP.

Ma et al. [3]. Furthermore, it is found that when modelling S_{SF} as an immersed boundary, the accuracy of the solution is somewhat insensitive to the vertical position where S_{SF} intersects the cell. As a general rule for an arbitrary free-surface marker, it is recommended to estimate $\nabla\varphi$ using a cell where the marker has local coordinates $\overline{x} = \overline{y} = 0$.

It was shown that solving the global hydrodynamic BVP in a NWT using an octree-grid technique to refine the grid locally near S_{SF} can lead to substantial improvements in the computational efficiency. An ambition of the present work is to utilize such improvements so that practical problems in marine hydrodynamics can be studied in a fully nonlinear framework without using supercomputers. Currently, the octree technique is being implemented in a time-domain solver where the grid is refined adaptively. We intend to present results from this work during the workshop.

5 Acknowledgments

This work was supported by the Research Council of Norway through the Centre of Excellence funding scheme, Project number 223254-AMOS and by DNV (formerly known as DNV GL).

References

[1] Finn-Christian W Hanssen, Andrea Bardazzi, Claudio Lugni, and Marilena Greco. Free-surface tracking in 2d with the harmonic polynomial cell method: Two alternative strategies. *International Journal for Numerical Methods in Engineering*, 113(2):311–351, 2018.

[2] Yan-Lin Shao and Odd M Faltinsen. A harmonic polynomial cell (hpc) method for 3d laplace equation with application in marine hydrodynamics. *Journal of Computational Physics*, 274:312–332, 2014.

[3] Shaojun Ma, Finn-Christian W Hanssen, Mohd Atif Siddiqui, Marilena Greco, and Odd M Faltinsen. Local and global properties of the harmonic polynomial cell method: In-depth analysis in two dimensions. *International Journal for Numerical Methods in Engineering*, 113(4):681–718, 2018.

[4] Hui Liang, Yun Zhi Law, Harrif Santo, and Eng Soon Chan. Effect of wave paddle motions on water waves. In *Proceeding of the 34th International Workshop on Water Waves and Floating Bodies, Newcastle, Australia*, 2019.